DEFORMATION AND STABILITY OF UNREINFORCED AND REINFORCED EMBANKMENT ON SOFT CLAY

W. Sae-Tia[1], M. Kouda[2], and O. Kusakabe[3]

ABSTRACT

The stability analyses of unreinforced and reinforced centrifuge model embankments of soft clay were carried out by using a limit equilibrium method and a plasticity solution. The unreinforced and reinforced embankments on soft clay foundation having undrained shear strength increasing with depth were constructed in a centrifuge. A parametric study was experimentally conducted in which the depth of the soft clay foundation was varied. The 2.5 m, 4.0 m and 8.0 m deep of soft clay foundation were modeled by Kawasaki Clay on which a sand embankment, modeled by Zircon sand, was constructed in-flight. The reinforcement restraints the lateral displacement of the soft clay foundation and reduces the lateral thrust in the embankment. The reduction of lateral thrust results in decreasing outward shear stresses and increasing inward shear stresses on the surface of soft clay, therefore the bearing capacity of the soft clay is improved. For long term behavior, the consolidation settlement is less affected by the reinforcement. The depth of soft clay has a marked influence on the failure mechanism of soft clay. It is recommended to use both limit equilibrium method and plasticity theory in order to obtain the required tension in geotextile and the profile of stresses along embankment base, respectively.

INTRODUCTION

In present day many techniques have been used to prevent the failure of embankment on soft clay. The short-term instability is the most critical condition, which takes place at the end of construction since the load is maximum whereas the strength of soil is minimum. To improve the stability of embankment, geotextile has been widely used over the past several years. A geotextile is used at the interface between embankment and soft clay foundation to enable the construction of embankment (Jewell, 1988; Terashi and Kitasume, 1988; Liu, et al., 1991; and Sera, et al., 1992). The geotextile can improve stability, decrease lateral displacements and allow embankments to be constructed to a greater height without the need of staged construction.

Embankment stability can be diminished if the foundation soil cannot adequately support the embankment. The failure of the foundation is assumed to occur as a result of one of two mechanisms, slip surface failure and bearing capacity failure (Bonaparte, et al., 1987; and Humphrey and Holtz, 1986). There are several methods that have been proposed for stability analyses of unreinforced and reinforced embankment on soft clay. Limit equilibrium analyses with a circular slip surface and plasticity solutions with a bearing capacity failure have been often assumed for stability analysis. The failure mechanisms of unreinforced and reinforced embankments on soft clay have been analyzed by several researchers and the influences of the depth and the increase in undrained shear strength with depth of soft clay foundation have been demonstrated (Jewell, 1988; Houlsby and Jewell, 1988; Low, et al., 1990; Michalowski, 1992; and Rowe and Mylleville, 1993).

In this paper, the stability of unreinforced and reinforced embankments by centrifuge modeling was examined by a limit equilibrium analysis and a plasticity solution. Firstly, the centrifuge test program and test procedures are briefly described. Secondly, from the results of centrifuge model tests, the effect of geotextile and the influence of the depth of soft clay are discussed. Thirdly, the stability analyses were carried out by the limit equilibrium method and the plasticity solution. Finally, the computed factor of safety and tensile force in geotextile are compared with the observed results from the centrifuge model tests.

1   Doctoral Student, Department of Civil Engineering, Hiroshima University, 1-4-1 Kagamiyama, Higashi-Hiroshima City, 739-8527, Japan.
2   Research Associate, Department of Civil Engineering, Tokyo Institute of Technology, 2-12-1 O-okayama, Meguro ku, 152-8552, Japan.
3   Professor, Department of Civil Engineering, Tokyo Institute of Technology, 2-12-1 O-okayama, Meguro ku, 152-8552, Japan.

CENTRIFUGE MODEL TEST

Test Conditions

To examine the change of the failure mechanism, the thickness of soft clay was varied. Six 1:100 scale centrifuge model tests were carried out using Mark III Centrifuge at Tokyo Institute of Technology. The typical set up of the centrifuge model test is shown in Fig. 1. A brief description of each test is given in Table 1. The natural marine clay of Kawasaki clay was used for model soft clay foundation. Its properties are as follows: liquid limit = 54%, plastic limit = 25.5%, plasticity index = 28.5, specific gravity = 2.69, compression index, C_c = 0.33, rate of strength increase $(C_u/\sigma')_{Ko}$ = 0.41 and void ratio under 1-D consolidation at 98 kPa = 1.045. For sand layer and sand embankment, the Zircon sand was used, which has a specific gravity of 4.66, the mean grain size, D_{50} = 0.18 mm and the friction internal angle from drained triaxial compression tests, ϕ_m = 38°. A nylon cloth, which has a comparable stress-strain relation with the prototype geotextile, was used as the model geotextile. The load transfer of soil-reinforcement was achieved by using five strain gages, which were glued on the model geotextile. The tensile strength of the instrumented model geotextile is 2.99 kN/m at ultimate tensile strain of 19.6%. The details of model geotextile, strain gages and the calibration of instrumented model geotextile can be found in the study by Sae-Tia, et al. (1998b).

Test Procedure

The details of the centrifuge model test can be found in the study by Sae-Tia, et al. (1998a). Only a brief explanation is mentioned here. Kawasaki clay was remolded and poured into a strongbox. Prior to pouring the clay, a drainage layer and a filter paper were laid down. The pressure was applied in three steps to obtain the designed surcharge pressures of 10 kPa on the surface of clay. Before the last loading step, five pore pressure and three earth pressure transducers were installed in the clay layer. The last pressure was maintained until consolidation reached 90%. The pressure was then removed and optical targets were placed on the frontal side surface of the model clay. Zircon sand was poured on the clay surface as a surcharge pressure of 10 kPa in flight. In the reinforced case, the model geotextile was laid down in this surcharge sand layer. Then four potential meters and a sand hopper were mount onto the strong box. The locations of all instruments are also shown in Fig. 1. The strongbox was placed on a centrifuge platform and was accelerated up to 100g. After consolidation was completed, the Zircon sand for embankment construction was poured in-flight from the sand hopper in six steps by 15 sec-time interval. During the construction, pore pressures, earth pressures, displacements and tensions were monitored. Photographs were taken at each step of construction. In the case of reinforced embankment, the tests continued until the clay reached the average degree of consolidation of 90%. Having stopped the centrifuge, moisture contents of clay foundation were measured at different locations in the clay layer.
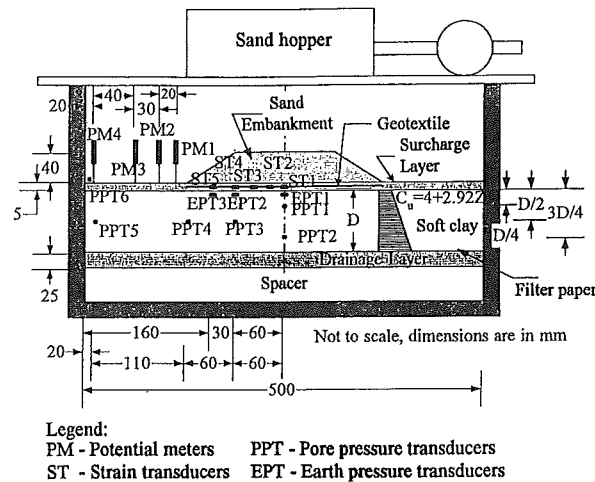
Table 1 Description of Each Centrifuge Model Test

Case. No.	Depth of soft clay, D (mm)	Reinforcement	Ratio of D/B, (B = mean width of embankment, 180mm)
WT-1	80 (8.0m in prototype scale)	Unreinforced	0.44
WT-4	40 (4.0m in prototype scale)	Unreinforced	0.22
WT-6	80	Reinforced	0.44
WT-7	40	Reinforced	0.22
WT-8	25 (2.5m in prototype scale)	Unreinforced	0.14
WT-9	25	Reinforced	0.14

B = mean width of embankment
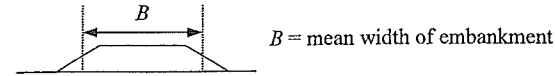
CENTRIFUGE TEST RESULTS

Effects of Reinforcement

Construction Pore Water Pressure

The 4 m height embankment was constructed in-flight in six steps; the total time to finish embankment was 120 seconds, which corresponds to two weeks in prototype. It was quite short time when compared with real construction process but it was done in such a way that it tries to ensure the undrained condition. Figure 2 shows the typical relations (WT-1, without geotextile) between excess pore pressure, Δu, and vertical pressure increment, $\Delta \sigma_v$, of two pore pressure transducers, 20 mm depth beneath the center of embankment (PPT1) and 40 mm deep beneath the toe of embankment (PPT4). The vertical stress increments were obtained from earth pressure transducer at the center of the embankment (EPT1). But in the cases of PPT4, the vertical pressure increments are calculated from an elastic stress distribution. The ratio of $\Delta u/\Delta \sigma_v$ at the center of embankment was nearly unity until the third layer of embankment and the excess pore pressure became almost constant with the increase in the vertical load increment. The ratio of $\Delta u/\Delta \sigma_v$ at the toe of embankment gradually increased during the construction and the ratio of $\Delta u/\Delta \sigma_v$ was about 1.67. Davies and Parry (1985) calculated the ratio of $\Delta u/\Delta \sigma_v$ from the centrifuge modeling of embankment on soft clay. They found that the ratios of $\Delta u/\Delta \sigma_v$ were 0.87 beneath the center of embankment and 1.91 beneath the toe of the embankment, which are quite similar to the values in this study. It can be explained that the excess pore pressure at the location further away from the centerline was generated by the horizontal stress as the principal stress direction rotated from vertical beneath the embankment centerline to near horizontal at beyond the toe.
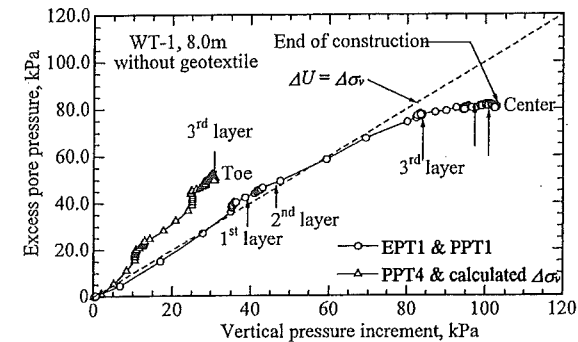

Fig. 1 General Arrangement of a Typical Centrifuge Model Test

Legend:
PM - Potential meters   PPT - Pore pressure transducers
ST - Strain transducers   EPT - Earth pressure transducers

Fig. 2 Relation Between Excess Pore Pressure and Vertical Pressure Increment of WT-1 Case

In the case of reinforced embankment (WT-6 test) at the same positions of transducers, the relations between excess pore pressures and vertical pressure increments are shown in Fig. 3. It can be seen that the ratio of $\Delta u/\Delta \sigma_v$ beneath the center was less than unity but the ratio beneath the toe was about unity. The ranges of value of $\Delta u/\Delta \sigma_v$ were 0.81 to 1.06 from the center of the embankment to the toe of the embankment. Rowe, et al. (1995) studied a full-scale test reinforced embankment and found that the maximum values of $\Delta u/\Delta \sigma_v$ beneath the center of embankment were 0.88 when the soil foundation approached to failure. The reason for this behavior is the geotextile supported part of the vertical load increment which lowered the vertical pressure increase in the soil foundation (Liu, et al., 1991). The results in this study are consistent with the previous observations.

Tension Induced in Geotextile

Figure 4 shows the typical induced tensions in geotextile and excess pore pressure with time for the cases of 8.0 m and 2.5 m depths of soft clay. In the deep layer, the induced tensions still increase after the construction corresponding with the pore pressures, which still increase after the completion of the embankment due to the redistribution of pore pressure from a zone of higher excess pressure to a zone of lower excess pressure. But in the case of 2.5 m, the induced tension decreases rapidly because the consolidation in shallow depth of soft clay takes place rapidly, compared with the deeper cases. Tensions in geotextile have been observed in both increase and decrease with time after the end of construction. This might be because there are two opposing factors: (1) consolidation of the foundation causes tension to decrease, and (2) lateral creep of the foundation that has the opposite effect (Rowe, 1982). For long-term behavior, the induced tension decreased with the increasing the consolidation process since the strength of soil increased during the consolidation. It should be noted that the induced tension at the center of the embankment (ST1) decreases rapidly at the initial state of consolidation and is almost constant even while the consolidation process is still taking place. The opposite trend is observed at the mid-slope where the induced tensions (ST5) are almost constant throughout consolidation process.

Displacement

The displacement of soft clay consists of two components, lateral and vertical displacements. Figure 5 shows the profiles of lateral displacement normalized by the depth of soft clay, δ_h/D, with normalized depth, z/D, beneath the mid-slope and the toe of the embankment at the end of construction. In the reinforced cases, the lateral displacements were significantly less than those of unreinforced cases. From Fig. 5, it indicates that the geotextile prevents the failure of embankment and causes the reduction of the lateral displacements. The reduction of lateral displacements depends upon the depth of soft clay, the smaller the depth, the greater the reduction. For all cases, the geotextile played less effect for the great depth than shallow depth of soft clay. In the case of 2.5 m, the normalized lateral displacement of the reinforced case at $z/D = 0.8$ was greater than that of the unreinforced case. It implies that the deformation zone or plastic region of reinforced cases was greater than those of unreinforced cases (Gourc, et al., 1986). For vertical displacement, the vertical displacement normalized by the depth of soft clay, δ_v/D, profiles along the horizontal direction, X-axis, at the end of construction of all cases were shown in Fig. 6. It is clearly seen that the geotextile plays less effect to the vertical displacements than the lateral displacement.

For long-term behavior, only the experiment of the reinforced case was carried out. Figure 7 shows the vertical displacements after average degree of consolidation of 90%. It is clear that the depth of soft clay is an important factor for governing the magnitude of vertical displacement. The greater the depth, the greater the displacement. Reinforcement has been shown theoretically to reduce differential settlement and lateral spreading of the embankment at the end of construction (Rowe, 1984). The opposite effect is that the reinforcement generally has little or no influence on consolidation settlement. Humphery and Holtz (1986) reviewed many reinforced embankment cases. For highway embankment in Africa, the reinforcement was reported to reduce lateral spreading of the embankment at the end of construction and consolidation settlement.

Effect of Foundation Depth on Deformation of Foundation

Figure 8 shows the correlation between normalized displacement at mid-slope with depth, δ/D, for both vertical and horizontal displacements with ratio of depth of soft clay and width of embankment, D/B. The reinforcement is effective in reduction of displacement in both directions, although the reductions in horizontal displacement were five times larger than vertical displacement. The reduced displacements due to the reinforcement depend on depth of soft clay. In the shallow depth of soft clay ($D/B = 0.14$), the reduced displacements are significantly larger than those of the deep cases ($D/B = 0.44$). It should be noted that the depth of soft clay has a less influence for the reinforced cases, compared with the cases of unreinforced embankments.
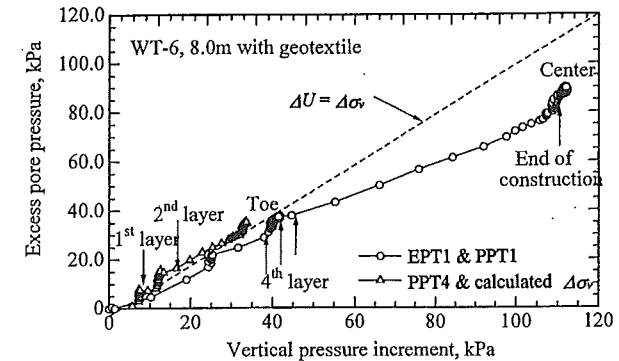

Fig. 3 Relation Between Excess Pore Pressure and Vertical Pressure Increment of WT-6 Case
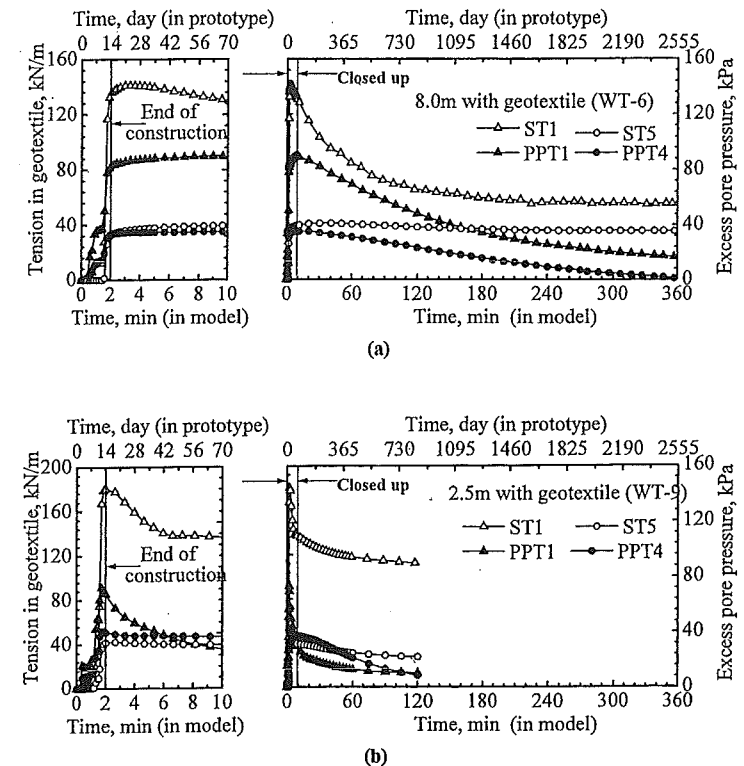

Fig. 4 Induced Tensions During Construction of Embankment and After (a) Consolidation, (b) Construction
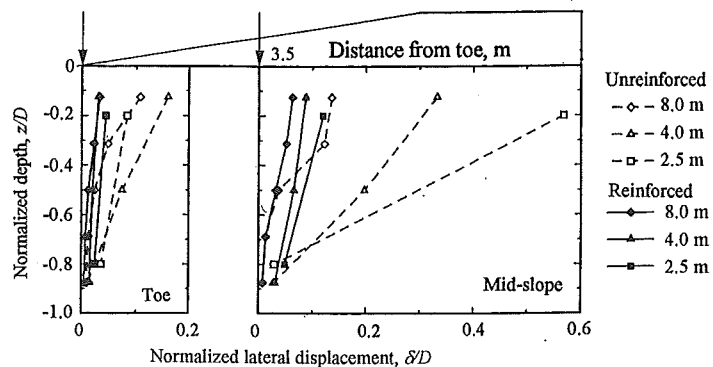
Fig. 5 Profile of Normalized Lateral Displacement with Normalized Depth
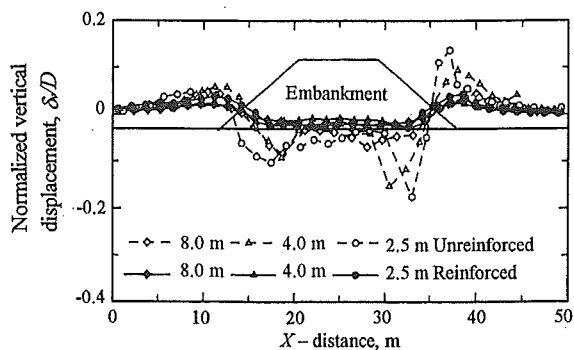

Fig. 6 Profile of Normalized Lateral Displacement along X-axis at the End of Construction
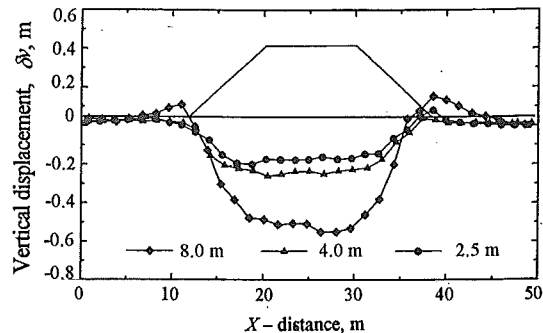

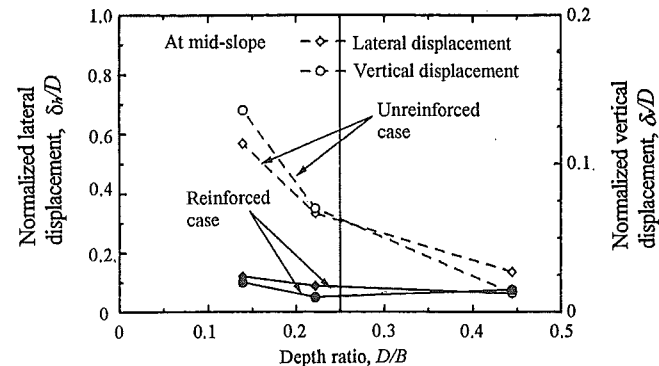Fig. 7 Profile of Vertical Displacement along X-axis after 90% of Consolidation

Fig. 8 Correlation Between Normalized Displacement by Depth and Depth Ratio

STABILITY ANALYSIS

Critical Height of Embankment

Figure 9 shows the relations between the maximum lateral displacements at the mid-slope of the embankment and the embankment heights respectively (based on unit weight of embankment being 21.4 kN/m³). The failure height (H_f) of the embankment can be determined from the intersection point of two straight lines extrapolated from the initial and final portions of the curve as shown in Fig. 9. The failure height (H_f) were 3.6 m, 4.5 m and 4.8 m for 8.0 m, 4.0 m and 2.5 m thickness of soft clay respectively (WT-1, WT-4 and WT-8).

Induced Tensions in Geotextile

In the reinforced cases, the embankments were constructed without failure because of the existence of the geotextile. The induced tensions in geotextile, T, and the strains along the horizontal direction (X-axis) are shown in Fig. 10, immediately after the completion of the embankment and after the degree of consolidation of 90% for two cases. The result from the case of reinforced 4.0 m depth of soft clay, WT-7, is not reported in this study since the earth pressure transducers were considered to malfunction. The maximum tensions were located at either the center or the shoulder of embankment, because the high shear strain developed near those areas in the soft clay. The maximum tensions force in the geotextile immediately after construction were 134.82 kN/m and 180.20 kN/m, which is equivalent to 6.1% and 8.2% of axial strain in the geotextile for a constant stiffness of 2200 kN/m in the cases of WT-6 and WT-9. Sharma (1994) studied the behavior of reinforced embankments on soft clay by centrifuge model test and found that the maximum tensions induced in reinforcement were located beneath the shoulder of the embankment.

Plasticity Theory

The stability of an embankment on soft clay can be calculated by plasticity theory since it can be determined as a bearing capacity problem. The plasticity theory allows the calculation of the maximum vertical stress that acts on a foundation with a surface shear stress. This is equivalent to a situation of embankment on soft clay. The embankment fill imposed vertical load to the foundation soil, equal to its weight, and the outward shear stress caused by the thrust in the embankment. The outward shear stress reduces the bearing capacity of the foundation soil. The reinforcement at the base of embankment can improve the stability of the embankment. The reinforcement supports the outward shear stress and provides inward shear stress on the surface of the foundation (Jewell, 1988). The reinforcement can be entered in the calculations by changing the direction of major principal stress on the surface of soft clay. The plasticity theory has been applied to calculate the limit vertical load of either unreinforced or reinforced embankments.
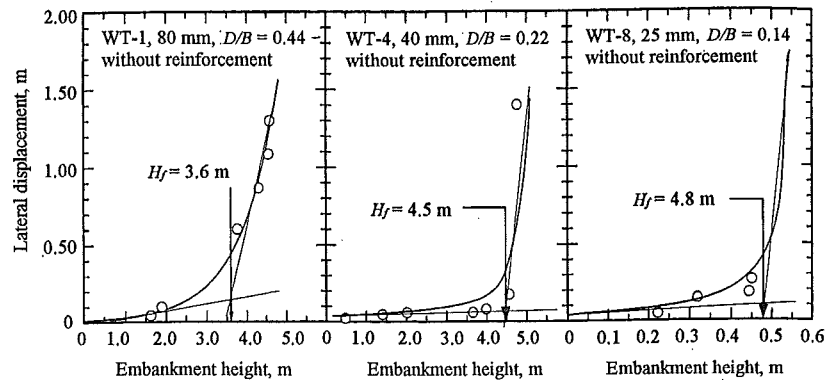
Fig. 9 Maximum Lateral Displacement Versus Embankment Height Curve for the Unreinforced Cases
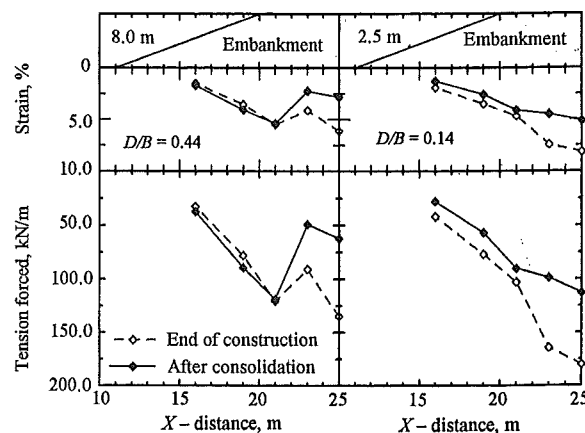

Fig. 10 Profiles of Induced Tension and Strain in Geotextile Along Embankment Base

The existing solutions are relevant to a foundation with undrained shear strength increasing with depth. In this study, the slip-line "Kotter equation" method has been used to calculate the bearing capacity of soft clay foundation under the undrained condition. The yield function of the cohesive soil is described by the equation as

$$F(\sigma_x, \sigma_z, \tau_{xz}) = \sqrt{(\sigma_x - \sigma_z)^2 + 4\tau_{xz}^2} - 2C_u = 0 \qquad (1)$$

where C_u = undrained shear strength of the soft clay foundation. The undrained shear strength is a function of depth z.

$$C_u = C_{uo} + kz \qquad (2)$$

where C_{uo} =   undrained shear strength at the top surface of the layer (kPa).
         k =   gradient of the strength with depth z (m).

The differential equilibrium equations are written as:

$$\partial\sigma_x/\partial x + \partial\tau_{xz}/\partial z = 0 \qquad (3)$$

$$\partial\tau_{xz}/\partial x + \partial\sigma_z/\partial z = \gamma \qquad (4)$$

where γ = unit weight of soil.

The above equations can be numerically solved using the slip line method. The typical network of characteristics of two cases, no shear stress and inward shear stress on the surface of foundation is presented in Fig. 11, showing that the deeper slip surface could form for the reinforced embankment and the bearing capacity increases.

In the unreinforced case, it is assumed that there is no shear stress on the surface of soft clay so that the direction of major principal stress, σ_p, is vertical ($\delta = 0°$). In the reinforced case, the inward shear stress occurs on the surface of soft clay so that the direction of σ_j is in the range 0° to 45° degree ($0 < \delta < 45$). The bearing capacity factor calculated, N_c, with the direction of major principal stress is shown in Fig. 12. For the fully reinforced case, $\delta = 45°$, the bearing capacity is improved by about 30% of the no shear stress, $\delta = 0°$, on the surface of soft clay.

The slip line method provides an advantage to allow more precise calculation of pressure distributions beneath the embankment, which are useful for the design of embankment on soft clay. The profiles of vertical pressure along the embankment base from plasticity theory and centrifuge model test are shown in Fig. 13 at the critical height for both unreinforced and reinforced cases. For the unreinforced cases, the calculated bearing capacity factor, N_c, is 16.53 so the maximum design height of embankment, H_{dmax}, becomes $N_c C_{uo}/\gamma = 16.53 \times 4/22 = 3.0$ m (66 kPa). Compared with the critical height 3.6m, 4.5m and 4.8m from centrifuge tests (WT-1, WT-4 and WT-8), the factors of safety, defined as $F_H = H_{dmax}/H_{cr}$, are 0.83, 0.67, and 0.65, respectively. For the reinforced cases, the inward shear stresses can be calculated from the measured induced tensions in centrifuge tests. The average direction of major principal stress from the centrifuge tests was found to be 5° (Sae-Tia, et al., 1998c). The bearing capacity factor is thus 17.76 ($\delta = 5°$) so the maximum design height of embankment is 3.3 m. In the fully reinforced case, $\delta = 45°$, the bearing capacity factor is 22.14 so the maximum design height becomes 4.0 m (88 kPa). The estimated maximum design height of embankment is quite small, compared with the actual embankment height about 5.0 m of the centrifuge test. It is probably because the depth of soft clay and effect of the surcharge sand layer are not taken into account in the analysis. Although the plasticity theory gives the small value of the maximum height however it generally gives a safe result for a design problem however. And also the foundation stability depends on the distribution of the applied surface stresses, not on maximum design pressure, $H_{dmax}\gamma$. As shown in Fig. 13, the calculated distribution of vertical stresses agrees well with those observed from the centrifuge tests.

Limit Equilibrium Equation

A simple and convenient procedure proposed by Low (1989) was used to calculate the factor of safety for embankment. This method assumes short term undrained response of the soft clay foundation and the failure surface is of circular slip surface. The expressions were obtained for the overturning moment M_o and the resisting moment M_R corresponding to an arbitrary slip circle that is tangent to a horizontal plane at a depth D_f below the top to the clay layer. The simplified section of the embankment in limit equilibrium analysis is shown in Fig. 14. The minimum factor of safety, F_s, is given by the equation:

$$F_s = N_1(C_A/\gamma H) + N_2[(C_m/\gamma H) + \lambda \tan\phi_m] \qquad (5)$$

where N_1 and N_2 =   stability numbers for the foundation and embankment respectively,
         λ =   coefficient of tan ϕ_m,
         γ =   unit weight of embankment,
         C_A =   average undrained shear strength within the depth D_f,
         D_F =   the trial limiting tangent depth,
         C_m =   undrained shear strength of embankment,
         ϕ_m =   friction angle of embankment, and
         H =   the height of embankment.

The details of derivations and the charts for determining the coefficients N_1, N_2 and λ should be referred to Low (1989). Their values depend on D_f/H and slope of embankment.
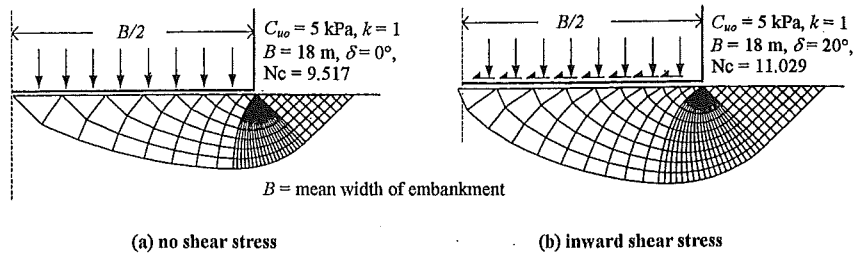
(a) no shear stress   (b) inward shear stress

Fig. 11 Typical Slip Line Network for the Case of No Shear Stress and Inward Shear Stress
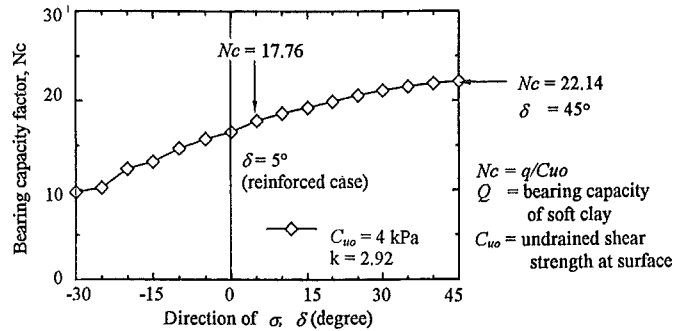

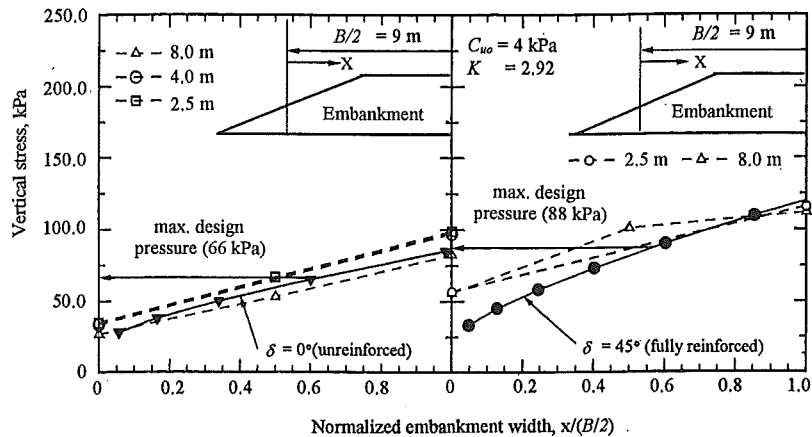**Fig. 12 Bearing Capacity of Soft Clay Based on Slip Line Method**
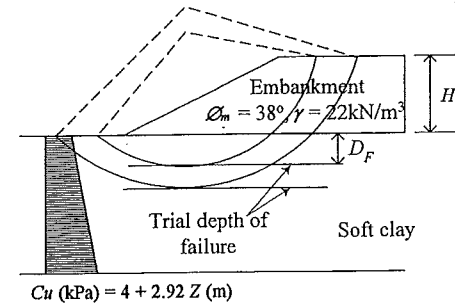

Cu (kPa) = 4 + 2.92 Z (m)

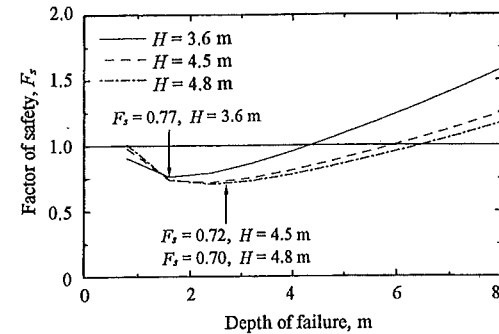**Fig. 14 Simplified Section of the Embankment in Limit Equilibrium Analysis**

Fig. 15 Relationship Between the Factor of Safety and Depth of Failure Surface

Figure 15 shows the relationship between the factor of safety with depth of failure surface. From the observed critical height 3.6 m, 4.5 m and 4.8 m from centrifuge tests, the calculated minimum factors of safety are 0.77, 0.72 and 0.70 for the cases of 8.0 m, 4.0 m and 2.5 m depth of soft clay respectively. The factors of safety are quite small probably because of the anisotropy of the undrained shear strength along the failure surface. The undrained shear strengths in compression and tension mode are different and influential on the predicted factor of safety and predicted failure thickness (Hanzawa, et al., 1980). Another possible reason is the increase of undrained shear strength of the soft clay due to partial consolidation during the construction period of the embankment.

In the case of reinforced embankment, when the force T acts where the critical slip circle intersects the base of the embankment, the factor of safety of the reinforced embankment with respect to rotational failure, F_R, can be calculated from the equation:

$$M_O = (M_S/F_R) + T(e/F_T) \qquad (6)$$

$$F_R = M_S/[M_O - T(e/F_T)] \qquad (7)$$

where M_S = resisting moment,
         M_O = overturning moment,
         F_R = overall factor of safety,
         F_T = safety factor of reinforcement, and
         e = lever arm of the force T.

Fig. 13 Profiles of Vertical Pressure Along the Embankment Base

The same procedure as is used in deriving the factor of safety for an unreinforced embankment was extended to calculate the force acting at the base of the embankment. The simple nonlinear equation for $T/\gamma H^2$ is obtained in terms of D_F/H, $\cot \beta$ and F_R/F_o:

$$(T/F_T) /\gamma H^2 = (D_F/H + 0.5) \{1 - [1-\eta \, (T/F_T)/(\gamma H^2)/a]^{0.32}/ (F_R/F_o)^{0.68}\} \quad (8)$$

where a = $(D_F/H + 0.5)^2/2 + (\cot^2\beta + 1)/24$,
        η = D_F/H when T is horizontal,
        $\cot \beta$ = slope of the embankment, and
        F_o = factor of safety for the unreinforced case.

The factor of safety F_R is a partial factor of safety, corresponding to the shear strength of soil. Therefore, the force T should be multiplied by a factor of safety, F_T, to get the tensile strength of the reinforcement T_u. The details of derivations are presented by Low, et al. (1990). From Eq. (8), the profile of required tension along the embankment base can be calculated by varying the depth of failure surface. The required tension at any point has to be less than the maximum available tension. The maximum available tension is the minimum of (1) the mobilized soil and reinforcement stress on each side and at each point along the reinforcement and the tensile strength of reinforcement material in the soil; and (2) the tensile strength of reinforcement material (Jewell, 1988). The maximum available tension along the embankment base is:

$$T_{max} = 2 \int_0^x \sigma_n \tan\phi_s \, dx \quad (9)$$

where T_{max} = maximum available tension force in kN/m,
        σ_n = normal pressure from embankment fill in kN/m², and
        $\tan \phi_s$ = friction coefficient between reinforcement and soil.

The interface friction angle, ϕ_s, has been calculated from direct shear tests between model geotextile and sand embankment, which equals to 14.4° (Sae-Tia, et al., 1998c).

The maximum required tensions were calculated from Eq. (8) at varied position on embankment base by equating F_R and F_T being unity. Figure 16 shows the maximum available tension force along the embankment from Eq. (9) by solid line, the maximum required tension from Eq. (8) by dash line and the tensile strength of model reinforcement 299 kN/m at 19.6% of strain (in prototype scale) by dash-dot line. The maximum tensions of 134.82 kN/m (6.1% of strain) and 180.20 kN/m (8.2% of strain) from two cases of centrifuge test are also shown in Fig. 16 by solid dot. The observed maximum tensions from the centrifuge tests show good agreement with the computed required tension from Eq. (8). For the case of 8.0m depth of soft clay (WT-6), the factor of safety for reinforcement, F_T, is 299/134.82 = 2.22 and the overall factor of safety, F_R, from Eq. (7) is 1.25. For the case of 2.5 m depth of soft clay (WT-9), the factor of safety for reinforcement, F_T, is 299/180.20 = 1.66 and the overall factor of safety, F_R, is 1.22.

Comparison of Failure Surface

From the photographic measurement, the failure surfaces were located. The vectors of displacement of all cases are shown in Fig. 17. For the unreinforced cases, the failure surfaces clearly developed after the completion of the embankment. The failure surface is close to a circular slip surface in the case of 8.0 m of soft clay. In the cases of 4.0 m and 2.5 m, the failure shapes are non-circular with large lateral displacement at the clay surface. In the reinforced cases, the failure does not occur but lateral displacements develop under the slope of embankment. It can be seen that the depth of soft clay strongly influences its deformation after the embankment construction. The analyzed failure surfaces of the unreinforced cases from the limit equilibrium analysis are also compared in Fig. 17.

From Fig. 17, the computed failure surfaces at minimum factors of safety are different from the observed failure surfaces. For the case of 8.0 m depth of soft clay, the computed failure surface is shallower than the observed failure surface. This may be caused by the partial drainage condition during the embankment construction, which would increase the strength of soft clay foundation. The trial failure surface, which has the factor of safety about unity (0.98), agrees well with the displacement vectors. For the shallow depth of foundation, the computed failure surfaces are deeper than the observed failure surfaces, probably because of the friction between the filter paper and the bottom of soft clay layer.

Although the limit equilibrium method gives a low minimum factor of safety and a different failure surface, it is noteworthy that it demonstrates the conservative design for overall stability. Moreover it provides a good prediction of the required tension in the reinforcement.
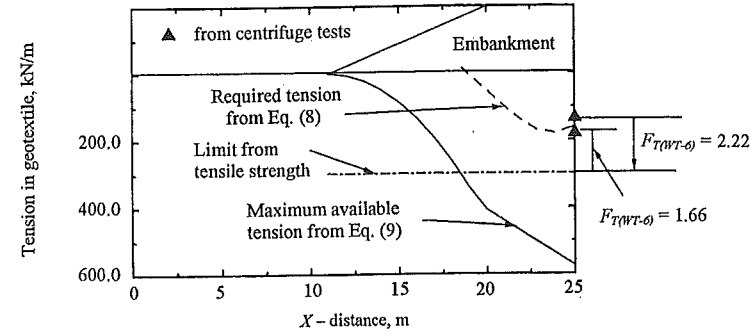

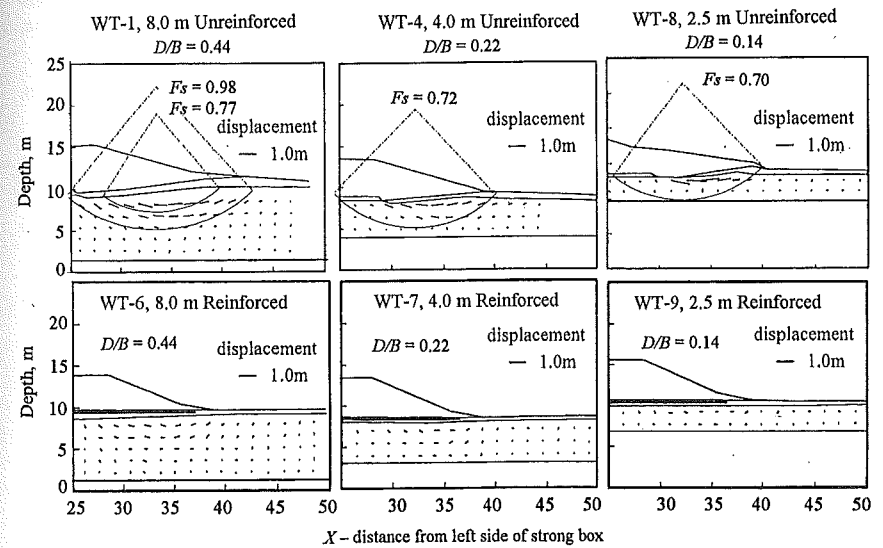Fig. 16 Profile of Available Tension in Geotextile Along the Embankment Base

Fig. 17 Displacement Vectors Immediately After Completion of the Embankment

CONCLUSION

From the centrifuge tests and stability analyses, the following conclusions can be drawn:

1. The reinforcement is effective to reduce significantly the lateral displacements in the soft clay and to carry the lateral thrust in the embankment.
2. The reduction of lateral thrust not only reduces outward shear stresses but also increases inward shear stresses on the surface of soft clay, therefore the bearing capacity of the soft clay is improved.
3. In the cases of unreinforced embankments, the depth of soft clay strongly influences the failure mechanism, which is clearly demonstrated by the lateral displacement profile. The smaller the depth, the greater the lateral displacement. In the cases of reinforced embankments, the depth of soft clay has an insignificant effect on lateral displacement since the failure did not occur for the same embankment height.
4. For long-term behavior, the effects of gain of strength in the soft clay due to the consolidation process reduce the tension force in the geotextile.
5. It is recommended to use both limit equilibrium method and plasticity theory for analyzing the unreinforced and reinforced embankment on soft clay. One of the advantages of plasticity theory is that it allows for calculation of the profile of stress along the embankment base. The limit equilibrium method has the advantage to predict the required tension in geotextile and overall stability.

REFERENCES

BONAPARTE, R.; HOLTZ, R.D.; and GIROUD, J.P. (1987). Soil reinforcement design using geotextiles and geogrids. *Proceedings of the ASTM Symposium on Geotextile Testing and the Design Engineer*. California, U.S.A., pp. 69-116.

DAVIES, M.C.R., and PARRY, R.H.G. (1985). Centrifuge modeling of embankments on clay foundations. *Soils and Foundations*, Vol. 25, No. 4, pp. 19-36.

GOURC, J.P.; MONNET, J.; and MOMMESSIN, M. (1986). Reinforced embankments on weak soil: Different theoretical approaches. *Proceedings of the Third International Conference on Geotextiles*. Vienna, Austria, pp. 1043-1048.

HANZAWA, H.; MATSUDA, E.; SUSUKI, K.; and KISHIDA, T. (1980). Stability analysis and field behavior of earth fills on and alluvial marine clay. *Soils and Foundations*, Vol. 20, No. 4, pp. 37-51.

HOULSBY, G.T., and JEWELL, R.A. (1988). Analysis of unreinforced and reinforced embankments on soft clays by plasticity theory. *Proceedings of Numerical Methods in Geomechanics*, pp. 1443-1448.

HUMPHREY, D.N., and HOLTZ, R.D. (1986). Reinforced embankment - A review of case histories. *Geotextiles and Geomembranes*, Vol. 4, pp. 129-144.

JEWELL, R.A. (1988). The mechanics of reinforced embankments on soft soil. *Geotextiles and Geomembranes*, Vol. 7, pp. 237-273.

LIU, LI-YU; WANG, MEI-RU; and DING, EN-RONG. (1991). Centrifugal tests of mechanism of geotextile-reinforced soft foundation under breakwater. *Centrifuge 91*, pp. 319-324.

LOW, B.K. (1989). Stability analysis of embankments on soft ground. *Journal of Geotechnical Engineering, ASCE*, Vol. 115, No. 2, pp. 211-227.

LOW, B.K.; WONG K.S.; LIM, C.; and BROMS, B.B. (1990). Slip circle analysis of reinforced embankments on soft ground. *Geotextiles and Geomembranes*, Vol. 9, pp. 165-181.

MICHALOWSKI, R.L. (1992). Bearing capacity of nonhomogeneous cohesive soil under embankments. *Journal of Geotechnical Engineering, ASCE*, Vol. 118, No. 7, pp. 1098-1118.

ROWE, R.K. (1982). The analysis of an embankment constructed on a geotextile. *Proceedings of the Second International Conference on Geotextiles*, Las Vegas, Nevada, U.S.A., pp. 677-682.

ROWE, R.K. (1984). Reinforced embankment: Analysis and design. *Journal of Geotechnical Engineering, ASCE*, Vol. 110, No. 1, pp. 231-246.

ROWE, R.K., and MYLLEVILLE, B.L.J. (1993). The stability of embankments reinforced with steel. *Canadian Geotechnical Journal*, Vol. 30, pp. 768-780.

ROWE, R.K.; GNANENDRAN, C.T.; LANDVA, A.O.; and VALSANGKAR, A.J. (1995). Construction and performance of a full-scale geotextile reinforced test embankment, Sackville, New Brunswick. *Canadian Geotechnical Journal*, Vol. 32, pp. 512-534.

SAE-TIA, W.; KOUDA, M.; and KUSAKABE, O. (1998a). Centrifuge modeling of unreinforced and reinforced embankment on soft clay. *Proceedings of Civil Engineering Seminar on Advanced Technology in Civil Engineering for Southeast Asian Regional Development*, Thailand, pp. 352-362.

SAE-TIA, W.; KOUDA, M.; and KUSAKABE, O. (1998b). Modeling of geotextile in a centrifuge model test. *Proceedings of the 53rd Annual Meeting of Japanese Society of Civil Engineering*, pp. 732-733.

SAE-TIA, W.; KOUDA, M.; KUSAKABE, O.; and TAKEMURA, J. (1998c). Observed behavior of reinforcement effect of woven sheet for embankment on soft clay in a centrifuge. *Journal of Geotechnical Engineering, JSCE*. Submitted for publication (in Japanese).

SERA, I.; MISHIMA, M.; TOYOMA, M.; and KAWAIDA, M. (1992). Model experiment on stability analyses of steel mesh reinforced embankment. *Proceedings of Earth Reinforcement Practice*, pp. 293-298.

SHARMA, J. (1994). Behavior of Reinforced Embankments on Soft Clay. Ph.D. Thesis, Cambridge University.

TERASHI, M., and KITAZUME, M. (1988). Behavior of fabric reinforced clay ground under an embankment. *Centrifuge 88*, pp. 243-252.